DYNAMIC MODELLING AND RESPONSE CHARACTERISTICS OF A MAGNETIC BEARING ROTOR SYSTEM INCLUDING AUXILIARY BEARINGS

April M. Free
George T. Flowers
Victor S. Trent

Auburn University
Auburn, AL 36849

Abstract

Auxiliary bearings are a critical feature of any magnetic bearing system. They protect the soft iron core of the magnetic bearing during an overload or failure. An auxiliary bearing typically consists of a rolling element bearing or bushing with a clearance gap between the rotor and the inner race of the support. The dynamics of such systems can be quite complex. It is desired to develop a rotordynamic model and assess the dynamic behavior of a magnetic bearing rotor system which includes the effects of auxiliary bearings. Of particular interest is the effects of introducing sideloading into such a system during failure of the magnetic bearing. A model is developed from an experimental test facility and a number of simulation studies are performed. These results are presented and discussed.

Nomenclature

C = damping, N–s/m
C_L = clearance of auxiliary bearing, m
D = nominal gap thickness, m
$\mathbf{F}_X$ = external force vector acting on the rotor in X direction, N
$\mathbf{F}_Y$ = external force vector acting on the rotor in Y direction, N
G = gravitational acceleration, m/s^2
I = rotor inertia matrix
i = current, amp
K = stiffness, N/m
k = gain value
L = equivalent circuit length
M = mass, kg
N = total number of modes considered
N_{B1} = node number at rotor left end
N_{B2} = node number at AMB
N_{B3} = node number at auxiliary bearing
N_{imb} = node number at imbalance location
N_T = number of turns of wire per coil
$\mathbf{Q}_X$ = rotor modal coordinate vector in X direction
$\mathbf{Q}_Y$ = rotor modal coordinate vector in Y direction
R_R = radius of rotor journal, m.
R_S = radius of auxiliary bearing bore, m.
t = time, s
t_f = fail time, s
v = voltage, volt
v_r = relative velocity at auxiliary bearing rotor/stator contact point
$\mathbf{X}_R$ = rotor physical coordinate vector in X direction
$\mathbf{X}_S$ = stator physical coordinate vector in X direction
$\mathbf{Y}_R$ = rotor physical coordinate vector in Y direction
$\mathbf{Y}_S$ = stator physical coordinate vector in Y direction
α = acceleration, rad/sec^2
δ = dynamic clearance
$\mathbf{\Gamma} = \mathbf{\Psi}^T\mathbf{I}\mathbf{\Psi}$
$\mathbf{\Phi}$ = rotor free-free modal displacement matrix
$\mathbf{\Psi}$ = rotor free-free modal rotation matrix
ψ = imbalance vector
μ_o = permeability of free space
μ_r = permeability of silicon steel
Ω = rotor operating speed, rad/s
τ = time constant
θ = angular position of the shaft
ζ = modal damping coefficient

Subscripts

a = first
B = auxiliary bearing
b = second
C = contact
g = gain constant
h = horizontal
l = left bearing
r = rate constant
v = vertical
x = x – direction
y = y – direction
bi = bias
1 = top magnet
2 = right magnet

3 = bottom magnet
4 = left magnet

Superscripts

a = current amplifier
c = controller
l = lead
p = sensor amplifier

Introduction

In recent years, the use of active magnetic bearings (AMB) for turbomachinery support has been an area of interest in both academia and in industry. Magnetic bearings provide the potential for significant improvements over other types of rotor supports, including elimination of wear, bearing friction-related energy losses and a means of actively suppressing rotor vibration. A critical feature of any magnetic bearing supported rotor system is auxiliary bearings to protect the soft iron core from rotor contact (and subsequent damage) during an overload or failure of the AMB. If the AMB fails partially, i.e. only one coil fails, the question arises to which is more advantageous: cutting off the AMB entirely or utilizing the remaining coils to aid in predicting the system response.

The present work is concerned with developing an understanding of the response characteristics of a rotor system supported by auxiliary bearings during failure of the AMB with and without use of sideloading. A design for an experimental test rig is presented and used as the basis for this study. A simulation model is developed in which response characteristics are studied and discussed.

Experimental Test Facility

The model and control system development presented in this study is for an experimental test facility. The apparatus consists of a radial magnetic bearing that is supporting the right end of a rotor. The left end of the rotor is supported by a ball bearing suspended in a frame by four springs. A photograph and the corresponding schematic diagram are shown in Figure 1.

The apparatus has two basic components: the rotor shaft and the magnetic bearing. The shaft is made of steel and is 0.0098 meters in diameter and 0.4572 meters in length. A steel disk of diameter 7.62 cm, thickness 2.54 cm, and mass 0.810 kg is placed at the midpoint of the bearing span. Threaded holes on the disk allow for imbalance to be added to the system.

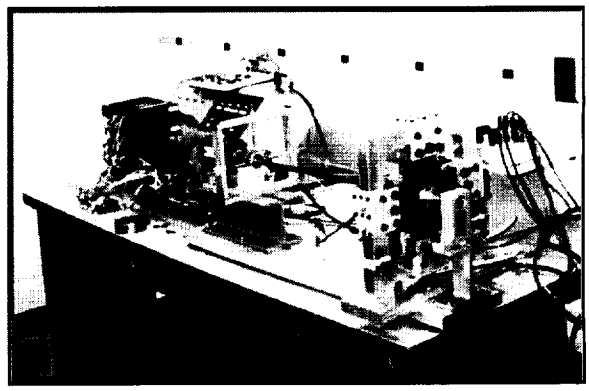

Figure 1.a Experimental Test Facility

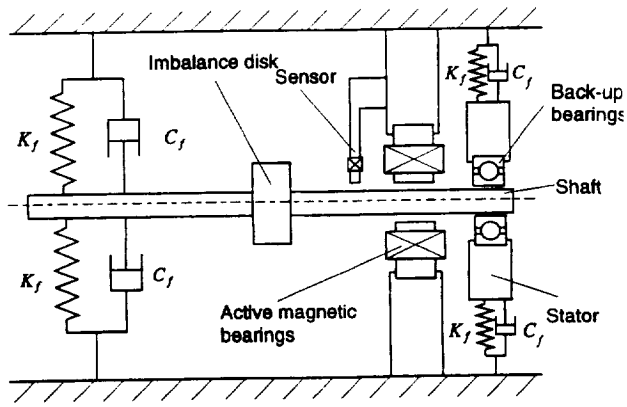

Figure 1.b Schematic Diagram of Experimental Test Facility

The rotor is driven by a variable speed motor. The speed of the rotor can be adjusted by turning the appropriate knob on the front panel of the control box. Shaft vibration is measured using eddy current proximity displacement sensors fixed to measure displacement in both the vertical and horizontal directions. The displacement signals are then sent to a signal analyzer.

The magnetic bearing is based upon a design described in Humphris, et al (1988). The basic parameters for the bearing are shown in Table 1. The bearing consists of four electromagnets equally spaced around a soft-iron core. A photograph and schematic diagram of the bearing are shown in Figure 2.

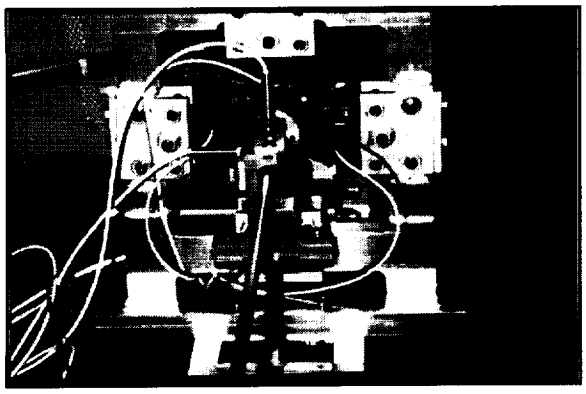

Figure 2.a Magnetic Bearing Assembly

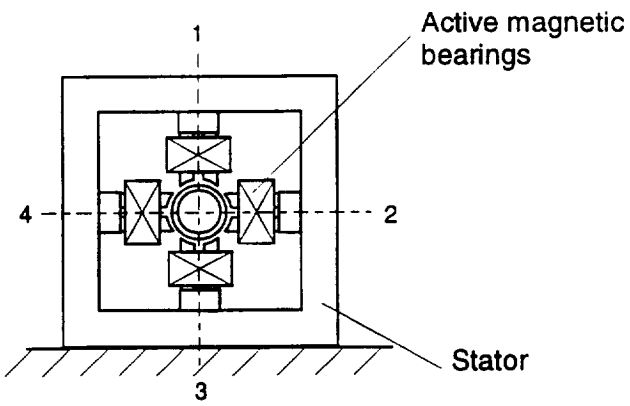

Figure 2.b Schematic Diagram of Magnetic Bearing

Simulation Model

A simulation model was developed for the rotor system described above. The model has three principal components – the rotor, magnetic bearing, and electronics. The governing equations for each are shown below.

The rotor is modelled using the free–free bending mode shapes and natural frequencies obtained through finite element analysis. The finite element code uses 11 stations and the first four modes (two rigid body and two flexible modes) are included in the simulation model. The rotor equations of motion can be expressed in terms of modal coordinates as

$$\ddot{\mathbf{Q}}_x + \Omega\Gamma\dot{\mathbf{Q}}_y + \omega_n^2\mathbf{Q}_x + \Phi^T\mathbf{F}_x = 0, \quad (1.a)$$

$$\ddot{\mathbf{Q}}_y - \Omega\Gamma\dot{\mathbf{Q}}_x + \omega_n^2\mathbf{Q}_y + \Phi^T\mathbf{F}_y = 0, \quad (1.b)$$

The auxiliary bearing consists of a ball bearing with a clearance between the rotor and the stator. The governing equations are

$$M_B\ddot{X}_B + C_{Bx}\dot{X}_B + K_{Bx}X_B = \mathbf{F}_{x,aux}, \quad (1.c)$$
$$M_B\ddot{Y}_B + C_{By}\dot{Y}_B + K_{By}Y_B = \mathbf{F}_{y,aux}, \quad (1.d)$$

where

$$\mathbf{F}_{x,lin}(N_{b1}) = \Phi_{N_{b1}}(K_{lx}\mathbf{Q}_x + C_{lx}\dot{\mathbf{Q}}_x)$$
$$\mathbf{F}_{y,lin}(N_{b1}) = \Phi_{N_{b1}}(K_{ly}\mathbf{Q}_y + C_{ly}\dot{\mathbf{Q}}_y)$$
$$\mathbf{F}_{x,imb}(N_{imb}) = \Omega^2\psi_6 cos\theta + \alpha\psi_6 sin\theta,$$
$$\mathbf{F}_{y,imb}(N_{imb}) = \Omega^2\psi_6 sin\theta - \alpha\psi_6 cos\theta,$$
$$\mathbf{F}_{x,aux}(N_{b3}) = \Phi_{N_{b3}}(\mathbf{F}_N cos\beta - \mathbf{F}_R sin\beta)$$
$$\mathbf{F}_{y,aux}(N_{b3}) = \Phi_{N_{b3}}(\mathbf{F}_N sin\beta + \mathbf{F}_R cos\beta)$$
$$\mathbf{F}_{grav} = \Phi^T MG$$
$$\mathbf{F}_N = \phi K_c(\delta - \mathbf{D}).$$

If $v_r = 0$, then $\mathbf{F}_R$ = required static friction force. If $v_r \neq 0$ or if required static friction force $> \mu_s\mathbf{F}_N$, then $\mathbf{F}_R = \mu_k\mathbf{F}_N$.

$$\mathbf{F_x} = \mathbf{F}_{x,lin} + \mathbf{F}_{x,imb} + \mathbf{F}_{x,aux} - \mathbf{F}_{x,amb}$$

$$\mathbf{F_y} = \mathbf{F}_{y,lin} + \mathbf{F}_{y,imb} + \mathbf{F}_{y,aux} - \mathbf{F}_{y,amb} + \mathbf{F}_{grav}$$

where

$$\sin(\beta) = \frac{\mathbf{Y}_R - \mathbf{Y}_S}{\sqrt{(\mathbf{X}_R - \mathbf{X}_S)^2 + (\mathbf{Y}_R - \mathbf{Y}_S)^2}},$$

$$\cos(\beta) = \frac{\mathbf{X}_R - \mathbf{X}_S}{\sqrt{(\mathbf{X}_R - \mathbf{X}_S)^2 + (\mathbf{Y}_R - \mathbf{Y}_S)^2}},$$

$$\delta = \sqrt{(\Phi\mathbf{Q}_x - X_b)^2 + (\Phi\mathbf{Q}_y - Y_b)^2},$$
$$\phi = 1 \; if \; \delta > \Delta$$
$$0 \; otherwise$$
$$\mathbf{Q}_x = \Phi^T\mathbf{X}_r,$$
$$\mathbf{Q}_y = \Phi^T\mathbf{Y}_r,$$

with

$$\mathbf{X}_r = \{X_{r1}, X_{r2}, \ldots, X_{rm}\}^T,$$
$$\mathbf{Y}_r = \{Y_{r1}, Y_{r2}, \ldots, Y_{rm}\}^T.$$

(m = total number of nodes)

The physical displacements of the rotor at the bearing and imbalance locations can be obtained using the following coordinate transformation:

$$X_{rk} = \sum_{i=1}^{N} \Phi_{ki} Q_{xi}, \qquad (k = N_{b1}, N_{b2}, N_{b3}, N_{imb})$$
$$Y_{rk} = \sum_{i=1}^{N} \Phi_{ki} Q_{yi},$$

The position of the shaft at the magnetic bearing location is measured using horizontal and vertical proximity sensors. They are modelled as linear first order systems.

$$\frac{dv_v^p}{dt} = \frac{k^p y - v_v^p}{\tau^p} \qquad (2.a)$$

$$\frac{dv_h^p}{dt} = \frac{k^p x - v_h^p}{\tau^p} \qquad (2.b)$$

The active control system is based upon a proportional–derivative (PD) control law and implemented using analog circuitry. The controller is modelled as

$$\frac{dv_v^c}{dt} = k_g v_v^p \tau^c + (k_g + k_r)\frac{v_v^p}{dt} - \tau^c v_v^c \qquad (3.a)$$

$$\frac{dv_h^c}{dt} = k_g v_h^p \tau^c + (k_g + k_r)\frac{v_h^p}{dt} - \tau^c v_h^c \qquad (3.b)$$

The control circuitry also includes a lead network. The governing equations are

$$\frac{dv_v^l}{dt} = \frac{1}{\tau_a^l} v_v^c + \frac{dv_v^c}{dt} - \frac{1}{\tau_b^l} v_v^l \qquad (4.a)$$

$$\frac{dv_h^l}{dt} = \frac{1}{\tau_a^l} v_h^c + \frac{dv_h^c}{dt} - \frac{1}{\tau_b^l} v_h^l \qquad (4.b)$$

Four current amplifiers (one for each coil) supply current to the magnetic bearing. They are modelled as

$$\frac{di_1^a}{dt} = -\frac{1}{\tau^a} i_1^a + \frac{1}{\tau^a} k_1^a v_v^l \qquad (5.a)$$

$$\frac{di_2^a}{dt} = -\frac{1}{\tau^a} i_2^a + \frac{1}{\tau^a} k_2^a v_v^l \qquad (5.b)$$

$$\frac{di_3^a}{dt} = -\frac{1}{\tau^a} i_3^a + \frac{1}{\tau^a} k_3^a v_h^l \qquad (5.c)$$

$$\frac{di_4^a}{dt} = -\frac{1}{\tau^a} i_4^a + \frac{1}{\tau^a} k_4^a v_h^l \qquad (5.d)$$

The forces supplied by the magnetic bearing to the rotor are assumed to be decoupled in the horizontal and vertical directions. The effects of flux saturation are included in the model based upon the approach described by Lewis (1993). The equations for these forces are

$$\mathbf{F}_{x,amb} = \mu_o A N_T^2 \left(\frac{i_2^2}{(2(D - x_{N_{B2}}) + \frac{L}{\mu_r})^2} - \frac{i_4^2}{(2(D + x_{N_{B2}}) + \frac{L}{\mu_r})^2} \right) \qquad (6.a)$$

$$\mathbf{F}_{y,amb} = \mu_o A N_T^2 \left(\frac{i_1^2}{(2(D - y_{N_{B2}}) + \frac{L}{\mu_r})^2} - \frac{i_3^2}{(2(D + y_{N_{B2}}) + \frac{L}{\mu_r})^2} \right) \qquad (6.b)$$

Discussion of Results

Using the rotordynamic model described in the preceding paragraphs, a study of the combined dynamics of a magnetic bearing supported rotor with

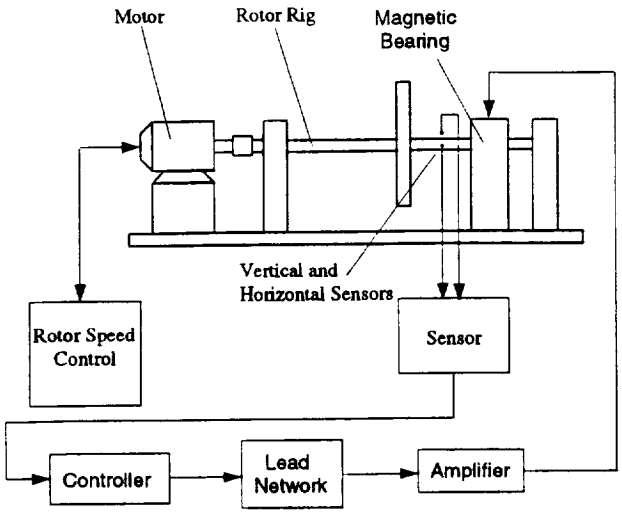

Figure 3 Block Diagram of Simulation Model

Parameter	Value	Units
K_{lx}, K_{ly}	17,510	N/m
C_{lx}, C_{ly}	2.0	N-s/m
K_C	87,557	N/m
C_C	0	N-s/m
K_B	17,510	N/m
C_{Bx}, C_{By}	2.0	N-s/m
M_B	0.033	kg
ψ_6	3.0×10^{-6}	kg-m
k^p	7.8×10^{3}	-
k_g	13	-
k_r	23	-
k^a	0.45	amp/v
τ^p	1.59×10^{-5}	-
τ_a^l	1.8×10^{-3}	-
τ_b^l	1.59×10^{-4}	-
τ^a	5.31×10^{-5}	-
A	3.42×10^{-4}	m^2
N_T	164	-
D	0.9×10^{-3}	m
μ_o	1.26×10^{-6}	-
v_1^b	4.2	volt
v_2^{bi}	1.9	volt
v_3^{bi}	1.0	volt
v_4^{bi}	1.9	volt

Table 1 Simulation Model Parameters

auxiliary bearings was performed. The parameters used in the simulation studies were identified from experimental evaluation of the test rig and are shown in Table 1. All of the responses illustrated in the figures are for this base parametric configuration, unlesss otherwise indicated. The rotor speed of 200 rad/sec was selected as a reasonable value above the first critical speed.

Figure 4 shows the rotor response without AMB failure. The horizontal and vertical responses are of the same amplitude and frequency at steady state. The response consists of a transient region of about 0.5 seconds in length followed by steady synchronous oscillations. As expected, the responses are similar to those for a conventionally supported rotor.

This study investigates the use of the three remaining coils of the AMB when one fails. By commanding the voltage of the controller, the attractive force, or sideloading of the remaining coils can be adjusted to help predict where the shaft will hit the auxiliary bearing and how it will behave once there is contact. This sideloading can be useful in providing stability to the system during partial failure of the AMB. The test configuration consists of allowing coil 2 to fail and investigating the effects of sideloading on the system. Coils 1 and 3 are kept in the same electronic configuration as if no failure had occurred. However, the voltage in coil 4 is set to a value that will pull the shaft horizontally over to the auxiliary bearing. Figures 5 through 7 show the rotor responses for failure of a single coil. Of interest in these figures is the influence of auxiliary bearing clearance and spin-down rate on the response characteristics. For the cases examined, the auxiliary bearing is quite stiff and the damping levels are quite low. For Figures 5.a - 5.c, the right coil of the AMB fails and all of the other coils remain active. Since the coupling between the horizontal and vertical motion is primarily through the gyroscopic terms, at steady state the vertical responses are little effected by the failure of the horizontal coil. It is observed that the responses may be quite high as the rotor bangs around on the auxiliary bearing, even with sideloading from the remaining coil. However, the sideloading is shown to be quite effective in encouraging rotor contact that will dissipate the vibrational energy. The response amplitudes tend to decrease as the auxiliary bearing clearance is decreased. However, a definite trade-off was encountered. If the clearance is too small, the rotor may strike the auxiliary bearing during steady-state operation if the imbalance is sufficiently high. This tends to unnecessarily perturb the rotor and shortens the life of the auxiliary bearing.

Figures 6.a - 6.c and 7.a - 7.c show the rotor behavior for spin-down at various rates. Again the response amplitudes tended to be lowest for smaller clearance values. However, an interesting

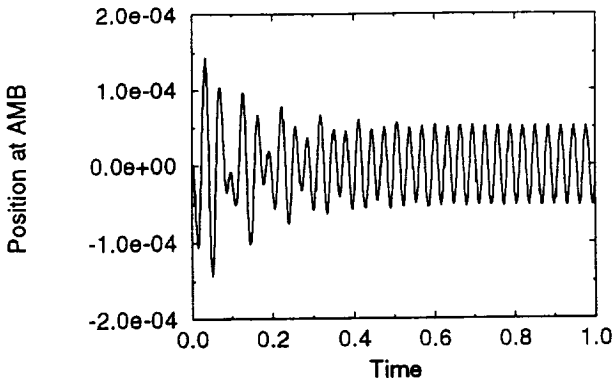

Figure 4 Rotor Response Without AMB Failure
$\Omega = 200\text{rad/sec}, C_L = \frac{D}{2}$

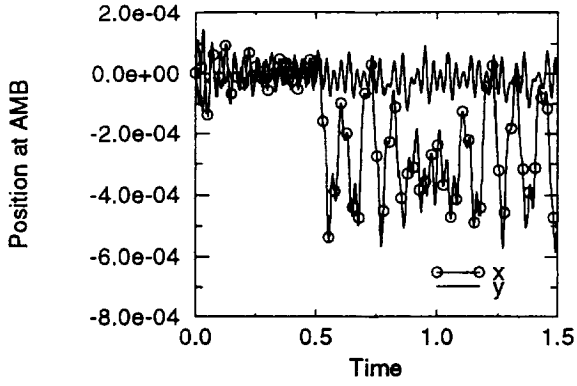

Figure 5.b Rotor Response With AMB Failure
$\Omega = 200\text{rad/sec}, C_L = \frac{D}{2}$
$t_f = 0.5, \alpha = 0$

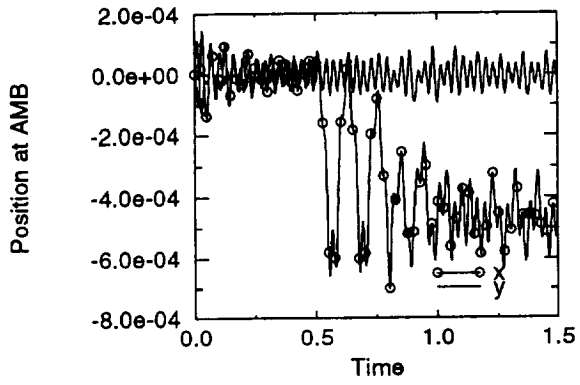

Figure 5.a Rotor Response With AMB Failure
$\Omega = 200\text{rad/sec}, C_L = \frac{2D}{3}$
$t_f = 0.5, \alpha = 0$

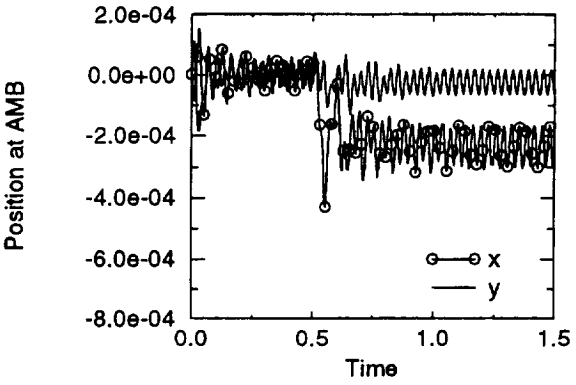

Figure 5.c Rotor Response With AMB Failure
$\Omega = 200\text{rad/sec}, C_L = \frac{D}{3}$
$t_f = 0.5, \alpha = 0$

behavior occurs as the rotor is spun down through the critical speeds. In each case, the highest amplitude responses are observed for the case with a clearance of $\frac{D}{2}$. For the higher and lower clearance values, the maximum amplitudes are lower. The effective stiffness for the $\frac{2D}{3}$ case is smaller, so the frequency of the transient vibrations is smaller.

An interesting phenomena is observed for the sideloading. The magnetic bearing forces are nonlinear functions of the dynamic clearance and the current. If one coil fails and the remaining coils are used to provide sideloading, the natural approach might seem to issue a constant command voltage, with the objective of having a constant sideloading force at steady state. However, the inherently unstable behavior of the magnetic bearing without active control coupled with the vibrational effects between the auxiliary bearing and the rotor, produces a severely unstable response. A remedy is to command a voltage that is proportional to the hor-

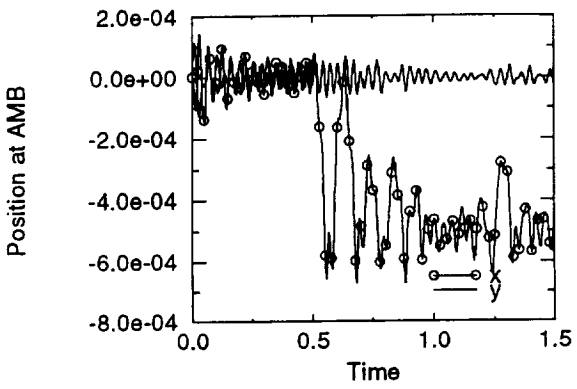

Figure 6.a Rotor Response With AMB Failure
$\Omega = 200\text{rad/sec}, C_L = \frac{2D}{3}$
$t_f = 0.5, \alpha = -50$

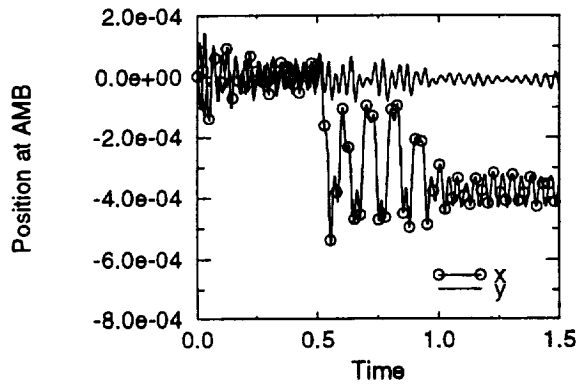

Figure 6.b Rotor Response With AMB Failure
$\Omega = 200\text{rad/sec}, C_L = \frac{D}{2}$
$t_f = 0.5, \alpha = -50$

izontal shaft displacement. Without an ideal amplifier, any value of desired sideloading force can be obtained with such a system. However due to the delay in the dynamics from the time constant of the power amplifier, unstable behavior may also result if the commanded voltage is too large. Figure 9 shows the maximum steady–state sideloading force that can be commanded with stable behavior as a function of power amplifier time constant. We see that a sufficiently low time constant will allow

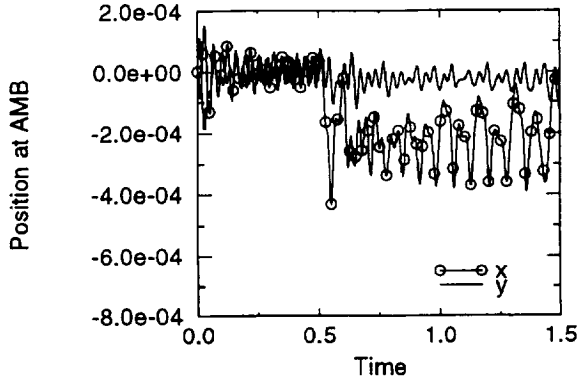

Figure 6.c Rotor Response With AMB Failure
$\Omega = 200\text{rad/sec}, C_L = \frac{D}{3}$
$t_f = 0.5, \alpha = -50$

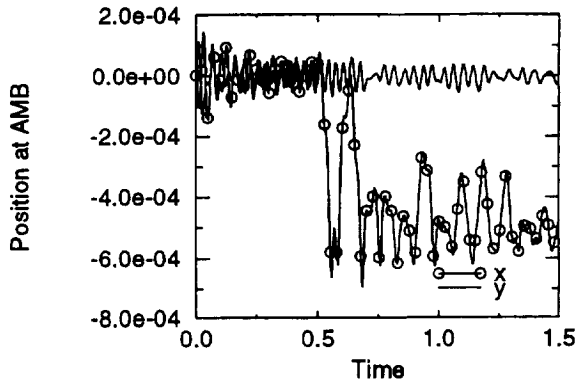

Figure 7.a Rotor Response With AMB Failure
$\Omega = 200\text{rad/sec}, C_L = \frac{2D}{3}$
$t_f = 0.5, \alpha = -100$

for virtually any desired level of sideloading.

Conclusion

A simulation model has been developed for a magnetic bearing supported rotor system with auxiliary bearings including frictional effects. The model has been described in detail with experimentally obtained model parameters. The re-

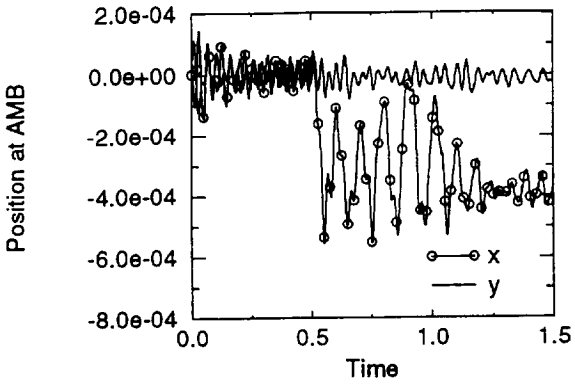

Figure 7.b Rotor Response With AMB Failure
$\Omega = 200\text{rad/sec}, C_L = \frac{D}{2}$
$t_f = 0.5, \alpha = -100$

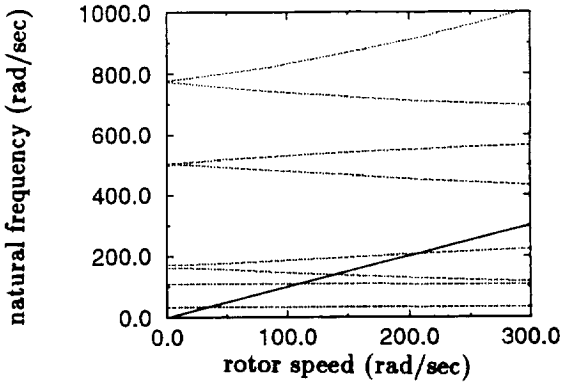

Figure 8 Rotor Natural Frequencies as a Function of Rotor Speed (for the parameters of Table 1)

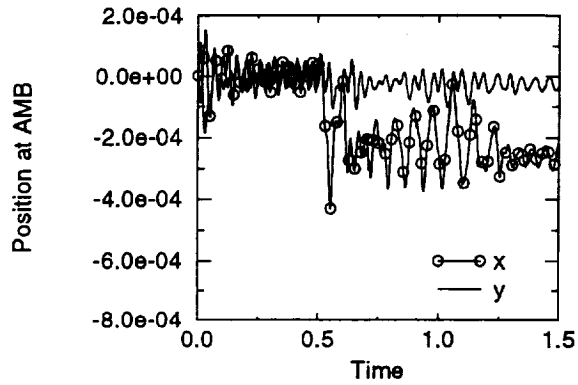

Figure 7.c Rotor Response With AMB Failure
$\Omega = 200\text{rad/sec}, C_L = \frac{D}{3}$
$t_f = 0.5, \alpha = -100$

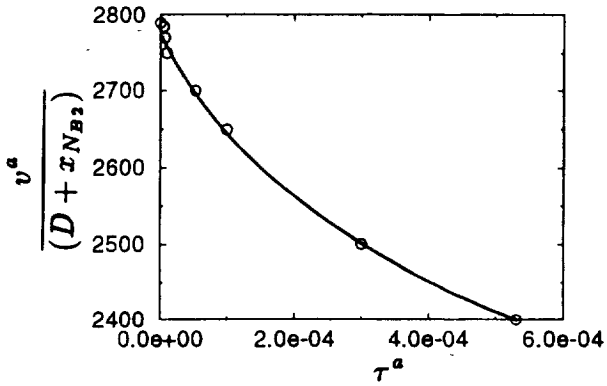

Figure 9 Maximum Sideloading Force as a Function of Power Amplifier Time Constant, τ^a (for parameters of Table 1)

sponse characteristics for a variety of auxiliary bearing clearances and spin-down rates are presented and discussed, including the effects of sideloading. In addition, some guidelines are given for the selection of appropriate levels of sideloading.

Acknowledgement

This work was partially supported by the National Aeronautics and Space Administration under Grant No. NAG3-1507. The Government has certain rights in this material. Special appreciation is expressed to Dr. Albert F. Kascak of NASA/Lewis Research Center.

References

Gondhalekar, V., and Holmes, R., "Design of a Radial Electromagnetic Bearing for the Vibra-

tion Control of a Supercritical Shaft," *Proceedings of the Institution of Mechanical Engineers,* Vol. 198C, No. 16, pp. 235–242.

Habermann, H., and Liard, G., "An Active Magnetic Bearing System," *Tribology International,* April, 1980, pp. 85–89.

Humphris, R.R., Kelm, R.D., Lewis, D.W., and Allaire, P.E., "Effect of Control Algorithms on Magnetic Journal Properties," *ASME Journal of Engineering for Gas Turbines and Power,* Vol. 108, October, 1986, pp. 624–632.

Ishii, T., Kirk, R.G., "Transient Response Technique Applied To Active Magnetic Bearing Machinery During Rotor Drop," *Rotating Machinery and Vehicle Dynamics,* Vol. 35, 1991, pp. 191–199.

Lewis, David W., "Electro and Permanent Magnet Materials," *Introduction To Magnetic Bearings: A Short Course,* July 27-28, 1993.

Shafai, B., Beale, S., LaRocca, and Cusson, E., "Magnetic Bearing Control Systems and Adaptive Forced Balancing," *IEEE Control Systems,* Vol. 14, No. 2, pp. 4–13.

Appendix – Linear Current and Position Stiffnesses

For design purposes, a linearized model for the magnetic bearing forces is needed.

The current stiffnesses are:

$$K_1^i = \frac{\mu_o A k_1^a v_1^{bi} N_T^2}{2D^2} \qquad (7.a)$$

$$K_2^i = \frac{\mu_o A k_2^a v_2^{bi} N_T^2}{2D^2} \qquad (7.b)$$

$$K_3^i = \frac{\mu_o A k_2^a v_2^{bi} N_T^2}{2D^2} \qquad (7.c)$$

$$K_4^i = \frac{\mu_o A k_2^a v_2^{bi} N_T^2}{2D^2} \qquad (7.d)$$

The position stiffnesses are:

$$K_1^P = \frac{\mu_o A (k_1^a v_1^{bi})^2 N_T^2}{2D^3} \qquad (8.a)$$

$$K_2^P = \frac{\mu_o A (k_2^a v_2^{bi})^2 N_T^2}{2D^3} \qquad (8.b)$$